Preprints.org

Article

Not peer-reviewed version

NIR-HSI/2B-CNN Algorithmic Scheme for Early Detection of Anthracnose on Mango Fruits

Thitima Phanomsophon , Panmanas Sirisomboon * , Jiraporn Sripinyowanich Jongyingcharoen , Apiwat Junto , Dharma Raj Pokhrel , Sneha Sharma , Jetsada Posom , Cheewanun Dachoupakan Sirisomboon * , Panan Rerngsamran , Pimpen Pornchaloempong , Norhashila Hashim , Anupun Terdwongworakul , Prabhas Chongstitvatana

Posted Date: 12 August 2024

doi: 10.20944/preprints202408.0759.v1

Keywords: mango; anthracnose; Colletotrichum asianum; near infrared; hyperspectral image; Convolutional Neural Network; CNN; Two Branch Convolutional Neural Network; 2B-CNN

Preprints.org is a free multidiscipline platform providing preprint service that is dedicated to making early versions of research outputs permanently available and citable. Preprints posted at Preprints.org appear in Web of Science, Crossref, Google Scholar, Scilit, Europe PMC.

Copyright: This is an open access article distributed under the Creative Commons Attribution License which permits unrestricted use, distribution, and reproduction in any medium, provided the original work is properly cited.

Preprints.org (www.preprints.org) | NOT PEER-REVIEWED | Posted: 12 August 2024 doi:10.20944/preprints202408.0759.v1

Disclaimer/Publisher's Note: The statements, opinions, and data contained in all publications are solely those of the individual author(s) and contributor(s) and not of MDPI and/or the editor(s). MDPI and/or the editor(s) disclaim responsibility for any injury to people or property resulting from any ideas, methods, instructions, or products referred to in the content.

Article

NIR-HSI/2B-CNN Algorithmic Scheme for Early Detection of Anthracnose on Mango Fruits

Thitima Phanomsophon [1], Panmanas Sirisomboon [2,*], Jiraporn Sripinyowanich Jongyingcharoen [2], Apiwat Junto [2], Dharma Raj Pokhrel [2], Sneha Sharma [3], Jetsada Posom [4], Cheewanun Dachoupakan Sirisomboon [5,*], Panan Rerngsamran [5], Pimpen Pornchaloempong [6], Norhashila Hashim [7,8], Anupun Terdwongwarakul [9] and Prabhas Chongstitvatana [10]

[1] Office of Administrative Interdisciplinary Program on Agricultural Technology, School of Agricultural Technology, King Mongkut's Institute of Technology Ladkrabang, Bangkok, Thailand
[2] Department of Agricultural Engineering, School of Engineering, King Mongkut's Institute of Technology Ladkrabang, Bangkok, 10520, Thailand
[3] Department of Infrastructure Engineering, The University of Melbourne, Victoria 3010, Australia
[4] Department of Agricultural Engineering, Faculty of Engineering, Khon Kaen University, 40002, Thailand
[5] Department of Microbiology, Faculty of Science, Chulalongkorn University, Bangkok, 10330 Thailand
[6] Department of Food Engineering, School of Engineering, King Mongkut's Institute of Technology Ladkrabang, Bangkok, Thailand
[7] Department of Biological and Agricultural Engineering, Faculty of Engineering, Universiti Putra Malaysia, Serdang 43400, Selangor, Malaysia
[8] SMART Farming Technology Research Centre (SFTRC), Faculty of Engineering, Universiti Putra Malaysia, Serdang 43400, Selangor, Malaysia
[9] Department of Agricultural Engineering, Faculty of Engineering at Kanpangsan, Kasetsart University, 74000, Thailand
[10] Department of Computer Engineering, Chulalongkorn University, Bangkok, 10330, Thailand
* Correspondence: panmanas.si@kmitl.ac.th and cheewanun.d@chula.ac.th

Abstract: This research proposes a near-infrared hyperspectral imaging/two-branch convolutional neural network (NIR-HSI/2B-CNN) algorithmic scheme to detect mango anthracnose of the species *Colletotrichum asianum* at the early stages of disease development. In the algorithmic model development, root mean square propagation was used as the solver to train the neural network, given 150 epochs. In addition, spectral raw data was preprocessed to transform it into an understandable and efficient format. The optimal classification model was the 2B-CNN model with 1st-derivative preprocessing, achieving an accuracy of 0.94 for the calibration set and 0.71 for the prediction set. The proposed NIR-HSI/2B-CNN scheme could detect anthracnose mangoes since the the first day of inoculation of the spore suspension (i.e., day 0) through to day 3, achieving a moderate classification accuracy. Meanwhile, the accuracy of conventional convolutional neural networks (CNN) were within a range of 0.66-0.67 for the calibration set and 0.55-0.57 for the prediction set. The results indicated that incorporating spatial features in the 2B-CNN modeling enhanced the prediction performance of the algorithm. The proposed NIR-HSI/2B-CNN algorithmic scheme needs refinements to be able to reliably sort mango fruits into those suitable for premium fresh consumption and export without anthracnose and those for domestic consumption or processing. The novelty of this research lies in the use of NIR-HSI and 2B-CNN algorithm to detect plant pathogens at the early stages of disease development. In addition, the new method of natural simulation to deposit the fungal spores onto the mango surface by spraying spore suspension onto the mango surface where the conidia penetrated unaided into the underneath of the mango peel is proposed.

Keywords: mango; anthracnose; *Colletotrichum asianum*; near infrared; hyperspectral image; Convolutional Neural Network; CNN; Two Branch Convolutional Neural Network; 2B-CNN

1. Introduction

© 2024 by the author(s). Distributed under a Creative Commons CC BY license.

Preprints.org (www.preprints.org) | NOT PEER-REVIEWED | Posted: 12 August 2024 doi:10.20944/preprints202408.0759.v1

Mango (*Mangifera indica* L.), hailed as the king of fruits [1–3], belongs to the *Anacardiaceae* family [4–6]. Originating in the Indian subcontinent around 4000 years ago, mango is regarded as an ancient tropical fruit, with hundreds of cultivars [7,8]. The fruit is cultivated in more than 90 countries in tropical and subtropical regions [9–11]. Mangoes rank fifth in global fruit production [11], with the annual global production of 57 million tons in 2021 [12]. Mango fruit is rich in nutrients, such as polyphenols, vitamins, and phytochemicals [13,14]. The health benefits of mango include antioxidants, anti-inflammatory properties, and anti-cancer potential.

Thailand is one of the world's leading producers and exporters of mangoes, particularly Nam Dokmai mangoes which are renowned for their sweetness, fragrant taste and smooth texture. The major overseas markets of Thai mango exports include China, Japan, European countries, the Middle East, and the United States. However, fresh mango exportation faces several challenges, including anthracnose which is a fungal disease affecting mangoes worldwide [15–17]. Ripe mangoes, including cv Nam Dokmai, are particularly vulnerable to infestation, affecting their quality and marketability.

Colletotrichum is a genus of plant pathogens that cause anthracnose diseases affecting mangoes and many other crops [16–20]. *Colletotrichum asianum* is one of the species of this genus known to cause anthracnose in mangoes [15–17,19,21]. Mango fruits are susceptible to infection at any point during their development. Infections on young fruits often result in mummification, while mature unripe fruits may show no visible symptoms [17,18,22]. Upon ripening, infected fruits typically exhibit small, water-soaked lesions on the surface, often turning brown or black, and become sunken as the disease advances [17,18,20]. After harvest and during transport of unripe mangoes, the anthracnose symptoms are usually not visible on the mango skin, but when the mangoes ripen, black spots or flecks will appear [23], which is undesirable to customers. As a result, early detection of anthracnose in mango fruit before symptoms appear is an effective method for controlling mango quality.

Mango anthracnose is caused by several species of fungus in the genus *Colletotrichum* [24]. In Thailand, *Colletotrichum gloeosporioides* and *Colletotrichum asianum* are the two most common species found in diseased mangos, particularly in the cultivar Nam Dokmai [17]. Both fungal species are nearly identical in terms of morphological characteristics such as colony color, development rate, and the size and form of appressoria and conidia. The aggressiveness exhibited by *C. asianum* and *C. gloeosporioides* on mango fruits was also similar, with a slight difference in color lesions where *C. asianum* produced dark brown spots and *C. gloeosporioides* produced lighter brown spots [25]. The disease of anthracnose in mango is caused by a series of sequential processes, including conidial germination, melanized appressoria formation, penetration of mango epidermis, and colonization of mango tissue when the spots start to appear. Specifically, conidia deposited on the surface of ripe mangos germinated after 12 hours, appressoria developed during 14-96 hours, and anthracnose symptoms started appearing at 5 days [25,26].

Visual inspection is commonly used to detect plant disease infections, including anthracnose diseases. However, inconsistencies often arise due to factors such as varying work conditions, subjective judgment, and worker fatigue [27]. Another approach involves identifying morphological atypical diseases (MAD) by assessing morphological features such as mycelial growth, conidia size, colony color, and texture. However, these features often fail to distinguish between different *Colletotrichum* species [28]. Meanwhile, image analysis techniques for identifying anthracnose on mangoes are only effective when lesions are visible [29]. As a result, a gap exists for a fast, non-destructive, and chemical-free method for early fungal infection detection, especially during the quiescent stage of development. Early detection enables the separation of infected mango, ensuring that mango export is of premium quality.

In [29], near-infrared hyperspectral imaging (NIR-HSI) in the spectral range of VIS-NIR (400-1000 nm) and machine learning (ML) algorithms were used to capture distinct spectral fingerprints of metabolites produced by *C. gloeosporioides* in mango fruits and tissue decomposition. The ML algorithms (i.e., principal component analysis and support vector machine) could detect anthracnose at early stages and accurately classify the extent of infection [29]. In [30], experiments

Preprints.org (www.preprints.org) | NOT PEER-REVIEWED | Posted: 12 August 2024 doi:10.20944/preprints202408.0759.v1

were carried out using five ML algorithms and NIR-HSI in the spectral range of VIS-NIR (480-950 nm) for early detection of mango anthracnose, and results were compared. The five ML algorithms included random forest (RF), quadratic discriminant analysis (QDA), XGBoost (XGB), simple perceptron (SLP), and multi-layer perceptron (MLP). The results showed that the MLP algorithm with full spectra achieved very high accuracy (0.961), along with other robust performance metrics including recall, specificity, F1 score, and Matthews correlation coefficient (MCC) [30]. In [31], further experiments were conducted using VIS-NIR-HSI (480-950 nm) and discriminant analysis ML algorithms for a comprehensive detection of anthracnose in mango fruits. The results showed that the QDA-powered classification model achieved the highest accuracy of 0.909 (i.e., QDA-full spectrum model with 54 variables), followed by the QDA-Correlation model with 27 variables (0.876) and the QDA-Tukey model with 20 variables (0.798) [31].

In theory, HSI preserves spatial information and can identify NIR absorptions at all locations in an image. Previous studies relied primarily on an average of spectra from all pixels in the image to create a prediction model, giving rise to noise and the loss of NIR absorption [20,30,31]. Unlike the conventional convolutional neural network (CNN), two branch convolutional neural network (2B-CNN) is a CNN model that utilizes both spectral data (averaged over all pixels) and spatial data (spectra in each pixel). Besides, anthracnose fungi naturally reside on certain locations of the mango peel, rather than covering the entire mango fruit. This fact renders 2B-CNN operationally ideal for classification of infected mango fruits. In addition, since 2B-CNN incorporates spatial data in the modeling process, the algorithm can be deployed to detect anthracnose on mango peel at the early stages of disease development.

Specifically, this research proposes a near-infrared hyperspectral imaging/two-branch convolutional neural network (NIR-HSI/2B-CNN) scheme to detect mango anthracnose of the species *C. asianum* at the early stages of disease development (i.e., before visible to the naked eye). In the experiment, disinfected mango fruits were sprayed with either *C. asianum* fungal spore suspension (i.e., to simulate fungal infections) or with sterile distilled water (control) prior to acquisition of NIR-HSI images. Furthermore, the classification performance of the proposed 2B-CNN model was compared with the CNN model.

2. Materials and Methods

2.1. Experimental Mango Fruits

The experimental mangoes were cv. Nam Dokmai sub cv. Sithong. An initial sample of 210 mango fruits were collected from six mango plantations in Thailand's eastern region (consisting of three orchards) and Central Plains (another three orchards), where Nam Dokmai mangoes are widely cultivated for export. In the sample collection, 30 mangoes were obtained from each orchard, with 1-5 mango fruits per mango tree and 10 mango trees per plantation. (Note: The sample collection was carried out twice for one orchard.) Essentially, there were seven batches of mango samples and each batch consisted of 30 mango fruits. All six plantations conform to the Thai Agricultural Standard for Mango (TAS 5-2015) [32]. The mangoes were collected 90 days after flower blooming, which is the commercial harvest period for mango fruits.

The mango fruits were disinfected by soaking in a bath at 55 °C for 5 min and in sterile cold water for another 5 min before drying in the laminar flow. In this study, slightly over half of the experimental mango fruits were excluded from the initial samples (210 mangoes) at the end of 11 days (or day 10) for the following reasons: (i) the mangoes developed stem rot; (ii) other plant diseases, rather than anthracnose, emerged; and (iii) anthracnose failed to develop following the deposition of fungal spore suspension. As a result, there were 99 mango fruits remaining for the algorithmic modeling.

2.2. Fungal Spore Suspension

Colletotrichum asianum extracted from anthracnose-infected mangoes was obtained from the Culture Collection Center of the Department of Microbiology, Faculty of Science, Chulalongkorn

Preprints.org (www.preprints.org) | NOT PEER-REVIEWED | Posted: 12 August 2024 doi:10.20944/preprints202408.0759.v1

University, Thailand. Spore suspension (1×10^5 conidia/mL) was prepared from *C. asianum* cultured on potato dextrose agar (PDA) plates at 25 °C for two weeks.

2.3. Fungal Deposition on Mango Fruits

To simulate the deposition of fungal spores onto healthy mango fruits, a sterile airbrush was used to spray the spore suspension on the mango fruits. Mango fruits in each of the seven batches of mango samples were first divided into five groupings (Groupings I – V) of six each. (Note: Each batch consisted of 30 mango fruits.) In each grouping, four mango fruits were sprayed with fungal spore suspension, while the other two mango fruits were sprayed with sterile distilled water using a sterile airbrush and served as control. Specifically, the mango fruits in Grouping I were sprayed once with fungal spore suspension or sterile water, twice for Grouping II, three, four, and five times for Groupings III, IV, and V, respectively.

The mango fruits were then individually placed in a transparent plastic container with lid to maintain high humidity and retained at room temperature for 11 days (i.e., days 0 – 10). The storage condition facilitated the natural ripening process and enabled the observation of disease development. In this study, the acquisition of NIR hyperspectral images of the mangoes was carried out from day 0 to day 10 (a total of 11 days) at the Department of Agricultural Engineering, Faculty of Engineering Kampangsang, Kasetsart University, Kampangsan campus. However, in this study, the NIR-HSI images of mango fruits taken at day 0 to day 3 (i.e., the first four days) of the final sampling of mango fruits (i.e., 99 mangoes) were used in the algorithmic modeling. The reason was that after day 3 the anthracnose symptoms were visible to the naked eye, thereby rendering the algorithmic model no longer necessary.

To quantify the fungal spores in Groupings I – V, the fungal spore suspension was sprayed onto PDA plates one, two, three, four, and five times, respectively, with three replications for each grouping. The PDA plates were then incubated at room temperature for 3 days before counting fungal colonies.

2.4. NIR Hyperspectral Image Acquisition

Figure 1 illustrates the schematic of the pushbroom near-infrared hyperspectral imaging (NIR-HSI) system with linear array of 320 CCD detectors (Xeva 992, Xenics Infrared Solutions, Belgium) and an imaging spectrograph (Imspector N17E Specim, Spectral Imaging Ltd., Oulu, Finland). The pushbroom system was used to acquire NIR-HSI images of the mangoes. The NIR-HSI system consisted of two 500-Watt tungsten-halogen light sources (Lowel Light Inc., New York, United States of America) positioned at an angle of 45° for uniform lighting in the field of view. The system was controlled by a desktop computer installed with Specim LUMO Software Suite (Spectral Imaging Ltd., Oulu, Finland).

In the NIR-HSI image acquisition, a transparent plastic container containing a mango sample (with the lid removed) was placed on the translation stage and scanned at a stage speed of 10 ms^{-1}. The white and dark references for background compensation were concurrently acquired with NIR-HSI images for radiometric correction. A Spectralon® reflectance material with a relative reflectance of 99% was used to capture the white reference, and the dark reference was automatically acquired by the NIR-HSI system by closing the camera shutter. Each NIR-HSI image in reflectance mode consisted of 256 spectral bands (12-bit color depth) between 900 and 1600 nm with a spectral resolution of 3.2 nm. The image of each band was 320 pixels in the x-direction (width) and n pixels (depending upon the length of the box) in the y-direction (length) [33]. The distance between the camera lens and the top surface of mango was approximately 30 cm, with a spatial resolution of 30 μm per pixel and the optimized integration time of 9 ms. After image acquisition, the raw hypercube was normalized using Eq. (1) to eliminate the instant noise due to the scanning background and the electronic drift of the detector.

$$R = \frac{R_s - R_d}{R_w - R_d} \quad (1)$$

Preprints.org (www.preprints.org) | NOT PEER-REVIEWED | Posted: 12 August 2024 doi:10.20944/preprints202408.0759.v1

where R is the relative reflectance image, R_s is the raw reflectance image, R_d is the dark reference image, and R_w is the white reference image.

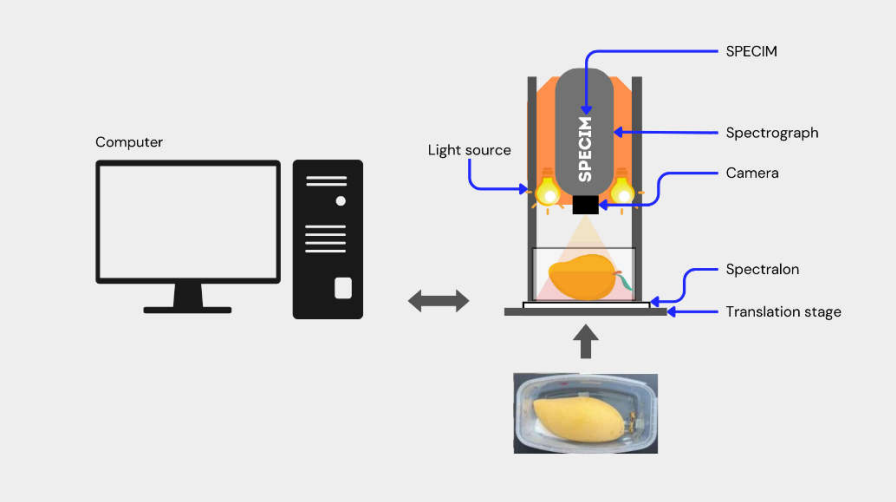

Figure 1. The experimental setup of the pushbroom near-infrared hyperspectral imaging (NIR-HSI) system.

2.5. Extraction of the Region of Interest

Hyperspectral imaging collects NIR absorption information from a sample in the form of images. As a result, preprocessing of NIR spectral data is required to remove physical phenomena in the spectra and to improve the performance of an algorithmic model. Specifically, a subset of an image must be selected to identify the region of interest (RoI) and exclude confounding regions. Figure 2(a) illustrates an NIR-HSI image prior to RoI extraction, consisting of a mango fruit, background, transparent plastic container, shadows, and moist cotton ball. This study followed the method in [34] with minor modifications to isolate the area of interest (i.e., mango fruit) from other regions (background, plastic container, shadows, and cotton ball). The mango fruits were identified by RGB color and wavelengths at 970 nm (related to H_2O [35]) and 1440 nm (related to sucrose [35]). Figure 2(b) shows the RoI-extracted image of mango fruit.

(**a**) (**b**)

Figure 2. (a) NIR-HSI image and (b) RoI-extracted image of mango fruit.

Preprints.org (www.preprints.org) | NOT PEER-REVIEWED | Posted: 12 August 2024 doi:10.20944/preprints202408.0759.v1

2.6. 2B-CNN Classification Modeling

A two-branch convolutional neural network (2B-CNN) is an extension of the convolutional neural network (CNN). Unlike CNN which utilizes either spectral or spatial information, 2B-CNN incorporates both spectral and spatial information in the classification modeling. In this research, the spectral branch of 2B-CNN was obtained by averaging the spectra of all pixels. In addition, to transform raw data into an understandable and efficient format, spectral preprocessing was carried out using different pretreatment techniques. The spectral preprocessing techniques being studied included baseline correction, mean centering, mean normalization, max-min normalization, Savitzky-Golay smoothing, standard normal variate (SNV), multiplicative scatter correction (MSC), first derivative (1D), and second derivative (2D). Meanwhile, the spatial branch was reduced to 25% of the original size, and the number of wavelengths was reduced from 256 wavelengths (900 – 1600 nm) to 10 principal components (PC) using principal component analysis (PCA). The reduction was necessary due to the large volume of data, thereby facilitating the model development.

In the algorithmic model development, the convolutional layers for 2B-CNN modeling followed Liu, *et al.* [36], with root mean square propagation (RMSProp) as the solver to train the neural network, given an epoch number of 150 and an initial learning rate of 0.001. Figure 3 shows the schematic diagram of the experimental design of this research. In the 2B-CNN modeling, the dataset (i.e., spectral and spatial data) were divided into the calibration (or training) dataset and prediction (or testing) dataset at a ratio of 80% to 20% using the Kennard-Stone method. There were a total of 396 datasets (i.e., 99 mango fruits × 4 days (day 0 – day 3)), consisting of 316 and 80 datasets for the calibration and prediction models, respectively. The training (calibration) dataset was used to develop the 2B-CNN classification model, and the testing (prediction) dataset was used to validate the classification model. Table 1 tabulates the convolutional layers of the 2B-CNN modeling.

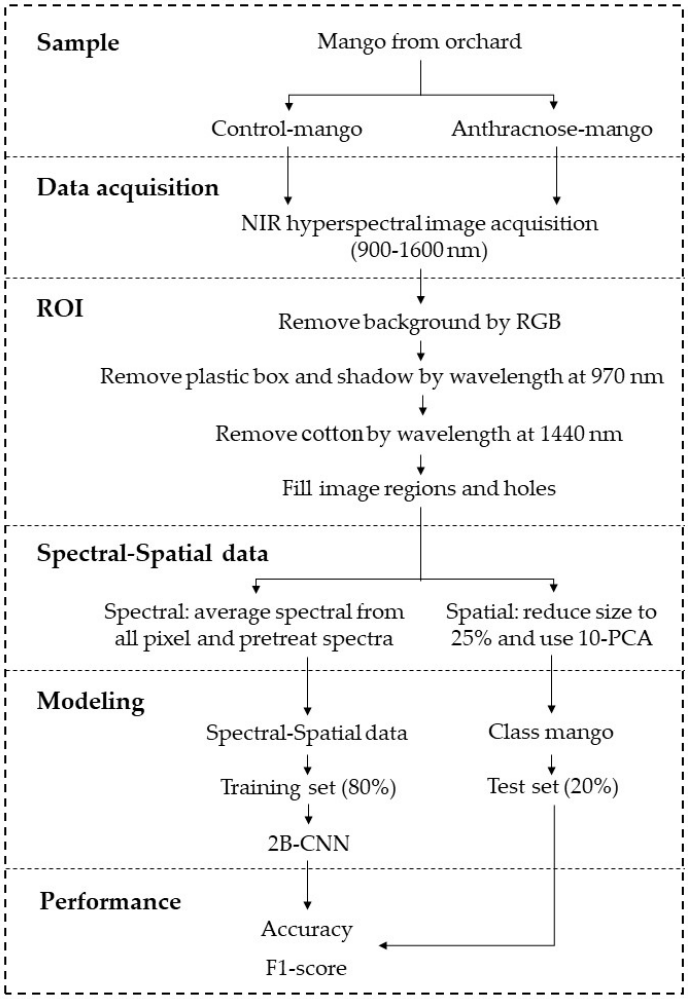

Preprints.org (www.preprints.org) | NOT PEER-REVIEWED | Posted: 12 August 2024 doi:10.20944/preprints202408.0759.v1

Figure 3. The experimental design diagram.

Table 1. The convolutional layers of 2B-CNN modeling [36].

2B-CNN (Full Spectra + Spatial)		
Spectral Branch (1D)	Conv1 (ReLU)	16x5
	Avg-pooling1	3
	Conv2 (ReLU)	16x5
	Avg-pooling2	3
	Conv3 (ReLU)	16x5
	Avg-pooling3	3
Spatial Branch (2D)	Conv4 (ReLU)	16x3x3
	Avg-pooling4	3x3
	Conv5 (ReLU)	16x3x3
	Avg-pooling5	3x3
	Conv6 (ReLU)	16x3x3
	Avg-pooling6	3x3
Fusion	Dropout	0.7
	SoftMax	-

2.7. Model Performance Metrics

In this study, the spectral raw data was preprocessed to transform it into an understandable and efficient format using various spectral pretreatment techniques, e.g., baseline correction, mean centering, and mean normalization. As a result, the performance of the 2B-CNN models with the various pretreatment techniques were compared, and the model with the best classification ability in terms of accuracy and F1 score was selected as the optimal classification model.

Accuracy is the proportion of correctly classified cases out of the total number of cases. The F1 score is the harmonic mean of precision and recall, where precision is the proportion of true positive predictions out of all positive predictions, and recall or sensitivity is the proportion of true positive predictions out of all actual positive cases. Figure 4 shows the confusion matrix and the performance metrics to evaluate the performance of the algorithmic models [37].

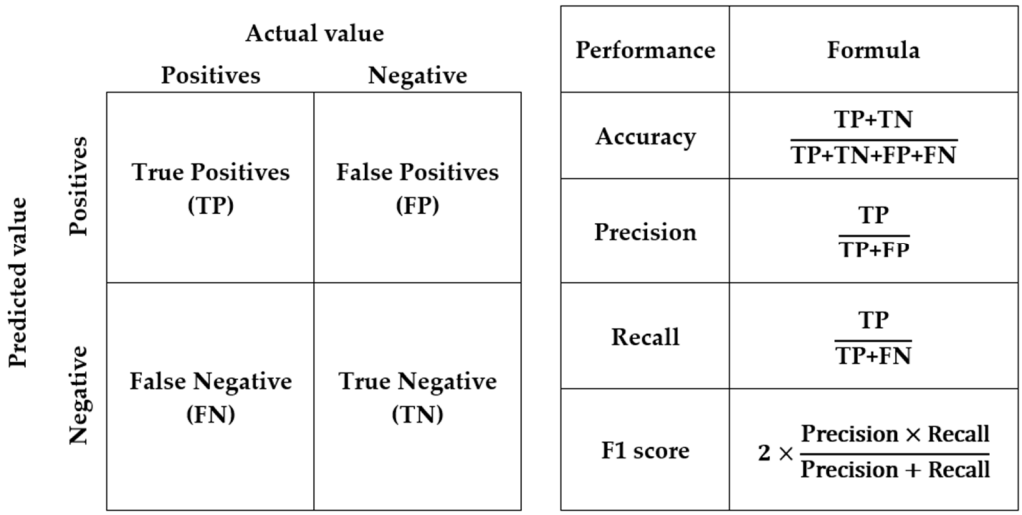

Figure 4. The confusion matrix and the performance metrics [37].

3. Results

The results indicated that the optimal classification model of mango fruits sprayed with anthracnose fungal suspension (i.e., infected mango) and with sterile water (non-infected mango or

Preprints.org (www.preprints.org) | NOT PEER-REVIEWED | Posted: 12 August 2024 doi:10.20944/preprints202408.0759.v1

control) was the NIR-HSI/2B-CNN algorithmic scheme with 1st derivative preprocessing, given 150 epochs. The classification accuracy of the optimal algorithmic scheme were 0.94 and 0.71 for the calibration and prediction models, respectively. Figure 5 shows the confusion matrix of the optimal 2B-CNN model with 1st derivative pretreatment.

Table 2 tabulates the classification performance of CNN and 2B-CNN algorithmic models with various spectral preprocessing techniques. The classification accuracy of the optimal 2B-CNN model with 1st-derivative pretreatment were 0.94 and 0.71 for the calibration and prediction models, respectively. The lower accuracy of the prediction set implied that more samples were required to improve the accuracy of the prediction set. In this current research, there were a total of 396 datasets, consisting of 316 and 80 datasets for the calibration and prediction models.

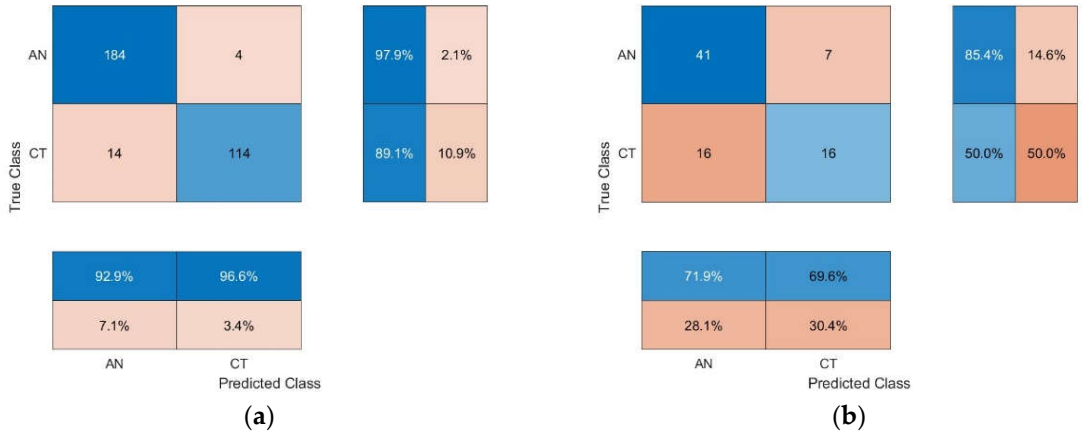

Figure 5. The confusion matrix of the optimal NIR-HSI/2B-CNN algorithmic scheme for classifying anthracnose-infected (AN) and non-infected (CT) mangoes: (a) calibration, (b) prediction.

In the calibration model, the precision, recall, and F1 score were 0.93, 0.98 and 0.95, respectively, for infected mangoes and 0.97, 0.89, and 0.93 for non-infected mangoes. Specifically, the precision indicated the extent to which the model can correctly classify true positive (TP) samples from the samples which were correctly (i.e., TP) and incorrectly classified (false positive or FP) as positive samples (i.e., TP+FP). The recall indicated the extent to which the model can correctly classify TP samples from all possible TP samples (i.e., TP+FN).

The results also showed that in the calibration set the ability of the 2B-CNN model to correctly classify samples as non-infected mangoes (not infected mangoes; precision = 0.93) was lower than its ability to correctly classify samples as infected mangoes (not non-infected mangoes; precision = 0.97).

The recall value indicated that the model could recognize non-infected mangoes (recall = 0.89) less than infected mangoes (recall = 0.98). The F1 score is the harmonic average of precision and recall, and it indicated the extent to which the model can correctly classify the TP samples. The F1 score ranges from 0 to 1, with higher values indicating better performance. In the calibration set, the F1 score of the model to correctly identify infected and non-infected mangoes were 0.95 and 0.93, respectively, suggesting that the calibration model was more capable of identifying infected mangoes than non-infected mangoes.

Meanwhile, in the prediction set, despite lower classification performance, the pattens were closely similar to the calibration model in that infected mangoes were identified more accurately than non-infected mangoes. In the prediction set, the recall for infected and non-infected mangoes were 0.85 and 0.50, respectively, and the corresponding F1 scores were 0.78 and 0.58. The precision values were almost the same (0.72 and 0.70 for infected and non-infected mangoes, respectively).

Furthermore, in the calibration model, the precision, recall, and F1 score for infected mangoes (0.93, 0.98, and 0.95, respectively) were slightly higher than those for non-infected mangoes (0.97, 0.89, and 0.93), indicating that the quantities of infected and non-infected mangoes in the calibration set were similar. However, in the prediction model, the recall and F1 score for infected mangoes (0.85 and 0.78) were higher than those for non-infected mangoes (0.50 and 0.58) because the quantity of

Preprints.org (www.preprints.org) | NOT PEER-REVIEWED | Posted: 12 August 2024 doi:10.20944/preprints202408.0759.v1

non-infected mangoes in the prediction set was much lower than infected mangoes, especially when compared to the calibration set. This led to overfitting which resulted in comparatively lower recall and F1 score.

The precision of the prediction model for infected mangoes (0.72) and non-infected mangoes (0.70) were slightly different, while the corresponding precision values of the calibration model were 0.93 and 0.97. However, in the prediction set, the recall and F1 score for infected mangoes (0.85 and 0.78) were considerably different from those for non-infected mangoes (0.50 and 0.58). This could be attributed to the fact that the precision was based on both TP and FP samples, which belonged to different groups, while the recall was based on only TP samples. The F1 score was based on both precision and recall, which were affected by both TP and FP samples but the effect of recall was more pronounced than the precision due to the TP effect. Since only TP samples were used in the calculation and given the substantially smaller quantity of non-infected mangoes, the TP effect on the recall and F1 score for non-infected mangoes of the prediction set was more evident than for infected mangoes.

Amirruddin, et al. [40] and Jensen [41] classified accuracy threshold into three categories: poor (less than 40.00%), moderate (40.00%-80.00%), and robust (more than 80.00%). Given the accuracy of 0.71, the proposed NIR-HSI/2B-CNN algorithmic scheme achieved moderate classification accuracy, and it can detect mango anthracnose at the early stages of disease development (i.e., day 0 – day 3) when the disease symptoms are not visible to the naked eye.

To improve the accuracy and F1 score, the dataset size should be increased for both the training (calibration) and testing (prediction) datasets. The current dataset size of 396 datasets was too small to effectively train and validate the algorithmic model. In addition, to reduce the model bias, the quantities of mango fruits infected by spraying with fungal spore suspension and with sterile water (non-infected) should be similar. The model bias was evident in a large disparity between the F1 score for infected (0.78) and non-infected mangoes (0.58). Furthermore, refinements should be made to the algorithms to improve the classification performance.

Meanwhile, given 150 epochs, the accuracy of the CNN model remained unchanged, independent of the spectral pretreatment methods. Given 1000 epochs, the CNN model with baseline correction (BL) spectral pretreatment achieved the highest classification accuracy of 0.66 and 0.75 for the calibration and prediction models, respectively. Given 10000 epochs, the CNN model with BL pretreatment achieved the highest accuracy of 0.67 and 0.78 for the calibration and prediction models. The results indicated that a substantial increase in epochs (i.e., from 1000 to 10000 epochs) had a negligible effect on the classification accuracy. However, a very large number of epochs could lead to data overfitting in prediction.

In comparison, the accuracy of the CNN model with BL pretreatment (0.66 and 0.75 for the calibration and prediction models) were lower than the proposed 2B-CNN model with 1st derivative preprocessing (0.94 and 0.71). The spectral pretreatment (i.e., 1st derivative for 2B-CNN and baseline correction for CNN) was carried out to reduce the baseline shift. Specifically, the spectra of NIR-HSI images of mango fruits suffered predominantly from baseline shift rather than radiation scattering in the mango fruit.

Table 2. Comparison between performance of 2B-CNN and CNN for classification of mango fruits sprayed with anthracnose (infected) and with water (non-infected).

model	epoch	Pretreatment	Calibration							Prediction						
			AC	Infected			Non-infected			AC	Infected			Non-infected		
				PC	RC	F1	PC	RC	F1		PC	RC	F1	PC	RC	F1
2B-CNN	150	raw	0.90	0.89	0.94	0.92	0.91	0.84	0.87	0.68	0.73	0.73	0.73	0.59	0.59	0.59
		BL	0.89	0.88	0.95	0.91	0.91	0.80	0.85	0.66	0.71	0.73	0.72	0.58	0.56	0.57
CNN	150	raw	0.66	0.66	0.66	0.66	0.66	0.66	0.66	0.75	0.75	0.75	0.75	0.75	0.75	0.75
		BL	0.66	0.66	0.66	0.66	0.66	0.66	0.66	0.75	0.75	0.75	0.75	0.75	0.75	0.75
	1000	raw	0.66	0.66	0.66	0.66	0.66	0.66	0.66	0.75	0.75	0.75	0.75	0.75	0.75	0.75
		BL	0.66	0.66	0.66	0.66	0.66	0.66	0.66	0.75	0.75	0.75	0.75	0.75	0.75	0.75
	10000	raw	0.67	0.67	0.67	0.67	0.67	0.67	0.67	0.78	0.78	0.78	0.78	0.78	0.78	0.78
		BL	0.67	0.67	0.67	0.67	0.67	0.67	0.67	0.78	0.78	0.78	0.78	0.78	0.78	0.78

Preprints.org (www.preprints.org) | NOT PEER-REVIEWED | Posted: 12 August 2024 doi:10.20944/preprints202408.0759.v1

		MC	0.92	0.94	0.93	0.94	0.90	0.91	0.91	0.65	0.71	0.71	0.71	0.56	0.56	0.56
		MN	0.88	0.86	0.95	0.90	0.92	0.77	0.83	0.70	0.73	0.79	0.76	0.64	0.56	0.60
		MMN	0.93	0.94	0.94	0.94	0.91	0.91	0.91	0.63	0.70	0.65	0.67	0.53	0.59	0.56
		SMT	0.58	0.94	0.31	0.46	0.49	0.97	0.65	0.45	0.61	0.23	0.33	0.40	0.78	0.53
		SNV	0.93	0.95	0.94	0.94	0.91	0.92	0.91	0.63	0.70	0.67	0.68	0.53	0.56	0.55
		MSC	0.94	0.94	0.96	0.95	0.94	0.91	0.92	0.58	0.65	0.63	0.64	0.47	0.50	0.48
		1D	**0.94**	**0.93**	**0.98**	**0.95**	**0.97**	**0.99**	**0.93**	**0.71**	**0.72**	**0.85**	**0.78**	**0.70**	**0.50**	**0.58**
		2D	0.51	0.95	0.19	0.31	0.45	0.98	0.62	0.49	0.82	0.19	0.31	0.43	0.94	0.59
CNN	150	**raw**	**0.59**	**0.59**	**1.00**	**0.75**	**-**	**0.00**	**-**	**0.60**	**0.60**	**1.00**	**0.75**	**-**	**0.00**	**-**
		BL	0.59	0.59	1.00	0.75	-	0.00	-	0.60	0.60	1.00	0.75	-	0.00	-
		MC	0.59	0.59	1.00	0.75	-	0.00	-	0.60	0.60	1.00	0.75	-	0.00	-
		MN	0.59	0.59	1.00	0.75	-	0.00	-	0.60	0.60	1.00	0.75	-	0.00	-
		MMN	0.59	0.59	1.00	0.75	-	0.00	-	0.60	0.60	1.00	0.75	-	0.00	-
		SMT	0.59	0.59	1.00	0.75	-	0.00	-	0.60	0.60	1.00	0.75	-	0.00	-
		SNV	0.59	0.59	1.00	0.75	-	0.00	-	0.60	0.60	1.00	0.75	-	0.00	-
		MST	0.59	0.59	1.00	0.75	-	0.00	-	0.60	0.60	1.00	0.75	-	0.00	-
		1D	0.59	0.59	1.00	0.75	-	0.00	-	0.60	0.60	1.00	0.75	-	0.00	-
		2D	0.59	0.59	1.00	0.75	-	0.00	-	0.60	0.60	1.00	0.75	-	0.00	-
	1000	raw	0.62	0.67	0.71	0.69	0.53	0.49	0.51	0.78	0.79	0.85	0.82	0.75	0.66	0.70
		BL	**0.66**	**0.71**	**0.72**	**0.71**	**0.58**	**0.56**	**0.57**	**0.75**	**0.74**	**0.90**	**0.81**	**0.73**	**0.53**	**0.63**
		MC	0.59	0.59	1.00	0.75	-	0.00	-	0.60	0.60	1.00	0.75	-	0.00	-

Preprints.org (www.preprints.org) | NOT PEER-REVIEWED | Posted: 12 August 2024 doi:10.20944/preprints202408.0759.v1

	MN	0.59	0.59	1.00	0.75	-	0.00	-	0.60	0.60	1.00	0.75	-	0.00	-
	MMN	0.59	0.59	1.00	0.75	-	0.00	-	0.60	0.60	1.00	0.75	-	0.00	-
	SMT	0.60	0.65	0.72	0.68	0.51	0.44	0.47	0.76	0.75	0.90	0.82	0.78	0.56	0.65
	SNV	0.59	0.59	1.00	0.75	-	0.00	-	0.60	0.60	1.00	0.75	-	0.00	-
	MSC	0.59	0.59	1.00	0.75	-	0.00	-	0.60	0.60	1.00	0.75	-	0.00	-
	1D	0.59	0.59	1.00	0.75	-	0.00	-	0.60	0.60	1.00	0.75	-	0.00	-
	2D	0.59	0.59	1.00	0.75	-	0.00	-	0.60	0.60	1.00	0.75	-	0.00	-
10000	raw	0.69	0.71	0.80	0.75	0.64	0.53	0.58	0.65	0.67	0.81	0.74	0.59	0.41	0.48
	BL	**0.67**	**0.70**	**0.79**	**0.74**	**0.62**	**0.50**	**0.55**	**0.78**	**0.76**	**0.92**	**0.83**	**0.72**	**0.56**	**0.67**
	MC	0.59	0.59	1.00	0.75	-	0.00	-	0.60	0.60	1.00	0.75	-	0.00	-
	MN	0.59	0.59	1.00	0.75	-	0.00	-	0.60	0.60	1.00	0.75	-	0.00	-
	MMN	0.59	0.59	1.00	0.75	-	0.00	-	0.60	0.60	1.00	0.75	-	0.00	-
	SMT	0.68	0.69	0.83	0.75	0.64	0.45	0.53	0.69	0.73	0.77	0.75	0.62	0.56	0.59
	SNV	0.59	0.59	1.00	0.75	-	0.00	-	0.60	0.60	1.00	0.75	-	0.00	-
	MSC	0.59	0.59	1.00	0.75	-	0.00	-	0.60	0.60	1.00	0.75	-	0.00	-
	1D	0.59	0.59	1.00	0.75	-	0.00	-	0.60	0.60	1.00	0.75	-	0.00	-
	2D	0.59	0.59	1.00	0.75	-	0.00	-	0.60	0.60	1.00	0.75	-	0.00	-

AC = accuracy, PC = precision, RC = recall, F1 = F1score, BL = baseline correction, MC = mean centering, MN = mean normalization, MMN = max-min normalization, SMT = Savitzky-Golay smoothing, SNV = standard normal variate, MSC = multiplicative scatter correction, 1D = first derivative, and 2D = second derivative.

4. Discussion

The 2B-CNN algorithm is superior to several machine learning or deep learning algorithms because 2B-CNN entails two branches, with one branch for spectral analysis and the other for spatial analysis. Such characteristics enable effective feature extraction and enhanced performance in tasks such as HSI classification [36]. In [36], a 2B-CNN algorithmic model was proposed to classify herbal medicine (210 samples of Pinellia ternate and 203 samples of Arisaema consanguineum Schott), strawberry (152 bruised and 156 unbruised samples) and green coffee beans (220 Robusta samples

Preprints.org (www.preprints.org) | NOT PEER-REVIEWED | Posted: 12 August 2024 doi:10.20944/preprints202408.0759.v1

and 220 Arabica samples), achieving an average classification accuracy of 96.72%. In comparison, the accuracy of support vector machine (SVM), 1D-CNN, and gray-level co-occurrence matrix algorithms were 92.60, 92.58, and 93.83%, respectively.

The high prediction ability of 2B-CNN is useful for the early detection of plant diseases, allowing for timely and effective corrective action. Of particular concern is anthracnose which is a fungal disease that causes dark lesions on vegetables and fruits, such as such as olive [38], mango [17,29], and strawberry [39]. The fungal disease affects produce production before and after harvest, resulting in crop damage and economic losses.

In [38], 1D-CNN with ResNet101 architecture was used with VIS-NIR-HSI (450–1050 nm) to detect anthracnose in olive fruits at the early stages of disease development, where the experimental olives were inoculated either with the fungus or water (i.e., control). The result showed that the algorithmic model was effective in detecting infected olives, achieving the sensitivity (or recall) of 85% on day 3 and 100% afterward [38].

In [30], experiments were carried out using five ML algorithms and NIR-HSI in the spectral range of VIS-NIR (480-950 nm) for early detection of mango anthracnose and results compared. The five ML algorithms included random forest (RF), quadratic discriminant analysis (QDA), XGBoost (XGB), simple perceptron (SLP), and multi-layer perceptron (MLP). The results showed that the MLP algorithm with full spectra achieved very high accuracy (0.961), along with other robust performance metrics including recall, specificity, F1 score, and Matthews correlation coefficient (MCC) [30]. In [31], further experiments were conducted using VIS-NIR-HSI (480-950 nm) and discriminant analysis ML algorithms for a comprehensive detection of anthracnose in mango fruits. The results showed that the QDA-powered classification model achieved the highest accuracy of 0.909 (i.e., QDA-full spectrum model with 54 variables), followed by the QDA-Correlation model with 27 variables (0.876) and the QDA-Tukey model with 20 variables (0.798) [31]. However, the aforementioned studies were conducted by experimentally puncturing the surface of the fruits to inoculate fungus, which differed from conidial germination of anthracnose fungus in nature.

Specifically, this research is the first to integrate 2B-CNN algorithm with NIR-HSI to detect anthracnose disease symptoms on the surface of mangoes at the early stages of disease development (i.e., before the symptoms are visible to the naked eye). In the experiment, *C. asianum* spore suspension was sprayed onto the mango surface to simulate the deposition of fungal spores in nature where the conidia penetrated unaided into the underneath of the mango peel. The proposed 2B-CNN algorithmic model with 1st derivative spectral preprocessing was able to detect the anthracnose fungus from the first day of the deposition of fungus (i.e., day 0) through to day 3 of the experiment, achieving an average accuracy of 0.71 for the prediction model.

5. Conclusions

This research proposed an NIR-HSI/2B-CNN algorithmic scheme to detect anthracnose in cv. Nam Dokmai sub cv. Sithong mango fruits at the early stages of disease development. The proposed algorithmic scheme could detect anthracnose mangoes from the first day of inoculation of the spore suspension (i.e., day 0) through to day 3, achieving a moderate classification accuracy of 0.71 for the prediction model. In comparison, the early detection of anthracnose on mango peel of the 2B-CNN model is superior to the conventional CNN model. The superior detection performance of the 2B-CNN model could be attributed to the incorporation of spatial features in the modeling. Nonetheless, the proposed NIR-HSI/2B-CNN algorithmic scheme needs refinements to be able to reliably sort mango fruits into those suitable for premium fresh consumption and export without anthracnose and those for domestic consumption or processing. The anthracnose is categorized as a plant pathogen rather than a human or animal pathogen. In subsequent research, the number of samples or datasets should be increased synthetically or by collecting naturally for balanced sample sets, and refinements should be made to the algorithmic model by adjusting convolutional layers, loss functions, and/or regularization techniques to improve classification performance.

Preprints.org (www.preprints.org) | NOT PEER-REVIEWED | Posted: 12 August 2024 doi:10.20944/preprints202408.0759.v1

Author Contributions: Conceptualization, T.P., S.S.; J.P., P.S., J.S.J., C.D.S., P.R., P.P., A.T. and P.C.; methodology, T.P., A.J., P.S., J.S.J., C.D.S., P.R., P.P., A.T. and P.C.; software, T.P.; validation, J.P., and N.H.; formal analysis, T.P.; investigation, A.J.; resources, A.T. and P.S.; data curation, A.J. and T.P.; writing—original draft preparation, T.P., D.R.P., P.S., C.D.S., P.R., N.H. and A.T.; writing—review and editing, T.P., P.S., C.D.S., P.R. and A.T.; visualization, T.P.; supervision, P.S., J.S.J., C.D.S., P.R., P.P., A.T. and P.C.; project administration, P.S., J.S.J., C.D.S., P.R., P.P., A.T. and P.C.; funding acquisition, P.S., J.S.J., C.D.S., P.R., P.P., A.T. and P.C. All authors have read and agreed to the published version of the manuscript.

Funding: This research was funded by Thailand Science Research and Innovation (TSRI), National Research Council of Thailand (NRCT) and King Mongkut's Institute of Technology Ladkrabang, BANGKOK, Thailand, for the research on 'preliminary study on near infrared hyperspectral image and thermal image for rapid diagnostic of mango fruit anthracnose on tree and post harvesting' (Grant number RE-KRIS/FF66/42) and The APC was funded by School of Engineering, King Mongkut's Institute of Technology Ladkrabang, BANGKOK, Thailand.

Acknowledgments: Authors would like to thank Thailand Science Research and Innovation (TSRI), National Research Council of Thailand (NRCT) and King Mongkut's Institute of Technology Ladkrabang, BANGKOK, Thailand, for the research grant of 'preliminary study on near infrared hyperspectral image and thermal image for rapid diagnostic of mango fruit anthracnose on tree and post harvesting' (Grant number RE-KRIS/FF66/42).

References

1. Khan, A.U.; Choudhury, M.A.R.; Tarapder, S.A.; Maukeeb, A.R.M.; Ema, I.J. Status of Mango Fruit Infestation at Home Garden in Mymensingh, Bangladesh. *Current Research in Agriculture and Farming (CRAF)* **2020**, *1*, doi:http://dx.doi.org/10.18782/2582-7146.119.
2. R, M.; Singh, S.K.; Srivastav, M.; Kalia, V.; Sharma, N.; Kumar, C.; Singh, N. The Population dynamics of fruit flies and correlation matrix with weather and host variables in mango (Mangifera indica) orchards. *The Indian Journal of Agricultural Sciences* **2023**, *93*, doi:https://doi.org/10.56093/ijas.v93i10.138967.
3. Lebaka, V.R.; Wee, Y.-J.; Ye, W.; Korivi, M. Nutritional Composition and Bioactive Compounds in Three Different Parts of Mango Fruit. *International Journal of Environmental Research and Public Health* **2021**, *18*, 741, doi:https://doi.org/10.3390/ijerph18020741.
4. Maharaj, A.; Naidoo, Y.; Dewir, Y.H.; Rihan, H. Phytochemical Screening and Antibacterial and Antioxidant Activities of *Mangifera indica* L. Leaves. *Horticulturae* **2022**, *8*, 909, doi:https://doi.org/10.3390/horticulturae8100909.
5. Guo, M.; Wu, Y.; Zhang, Y.; Hu, S.; Jia, Y.; Luo, X. Nutritive value of active volatile components of Anacardiaceae mango and their effects on carrier proteins function. *Food Research International* **2023**, 112779, doi:https://doi.org/10.1016/j.foodres.2023.112779.
6. Derese, S.; Guantai, E.M.; Yaouba, S.; Kuete, V. Mangifera indica L. (Anacardiaceae). In Medicinal Spices and Vegetables from Africa: Therapeutic Potential Against Metabolic, Inflammatory, Infectious and Systemic Diseases; Elsevier Inc.: Cambridge, MA, USA, 2017; Volume 451–483.
7. Jenny, F.; Sultana, N.; Islam, M.M.; Khandaker, M.M.; Bhuiyan, M.A.B. A review on anthracnose of mango caused by Colletotrichum gloeosporioides. *Bangladesh Journal of Plant Pathology* **2019**, *35*, 65-74.
8. Ahmed, A.; Alam, M.J.; Momin, M.A.; Rahman, R.; Alam, K.M.; Islam, A.B.M.J.; Ali, M.M. Production performance of mango in dinajpur district of Bangladesh (A case study at sadar upazilla). *European Journal of Agriculture and Forestry Research* **2017**, *5*, 16-57.
9. Shankar, S.; Kumar, G.; Singh, A.; Mishra, P.K. Revealed comparative advantage (RCA) and its application to evaluate India's performance of fresh mangoes, mangosteen & guavas during the period 1991-2020: An analysis with respect to trade. *Journal of Contemporary Issues in Business and Government* **2023**, *29*, 105-111, doi: https://doi.org/10.47750/cibg.2023.29.01.030.
10. Saúco, V.G. Mango production and world market: Current situation and future prospects. *Acta Horticulturae* **2004**, *645*, 107-116, doi:https://doi.org/10.17660/ActaHortic.2004.645.7.
11. Padaliya, S.; Pundir, R.S. Challenges faced by mango exporters. *Gujarat Journal of Extension Education* **2022**, *34*, doi:https://doi.org/10.56572/gjoee.2022.34.2.0004.
12. Torgbor, b.B.A.; Rahman, M.M.; Brinkhoff, J.; Sinha, P.; Robson, A. Integrating Remote Sensing and Weather Variables for Mango Yield Prediction Using a Machine Learning Approach. *Remote Sensing* **2023**, *15*, 3075, doi:https://doi.org/10.3390/rs15123075.
13. Uddin, M.N.; Afroz, M.; Moon, N.J.; Shefat, S.H.T. Management of anthracnose disease of mango caused by Colletotrichum gloeosporioides: A review. *Acta Scientific* **2018**, *2*, 169–177.
14. Lauricella, M.; Emanuele, S.; Calvaruso, G.; Giuliano, M.; D'Anneo, A. Multifaceted health benefits of Mangifera indica L. (Mango): The inestimable value of orchards recently planted in Sicilian rural areas. *Nutrients* **2017**, *9*, 525, doi:http://dx.doi.org/10.3390/nu9050525.

Preprints.org (www.preprints.org) | NOT PEER-REVIEWED | Posted: 12 August 2024 doi:10.20944/preprints202408.0759.v1

15. Benatar, G.V.; Wibowo, A.; Suryanti. First report of Colletotrichum asianum associated with mango fruit anthracnose in Indonesia. *Crop Protection* **2021**, *141*, 105432, doi:https://doi.org/10.1016/j.cropro.2020.105432.
16. Tovar-Pedraza, J.M.; Mora-Aguilera, J.A.; Nava-Díaz, C.; Lima, N.B.; Michereff, S.J.; Sandoval-Islas, J.S.; Câmara, M.P.S.; Téliz-Ortiz, D.; Leyva-Mir, S.G. Distribution and pathogenicity of Colletotrichum species associated with mango anthracnose in Mexico. *Plant Disease* **2020**, *102*, 137-146, doi:https://doi.org/10.1094/PDIS-01-19-0178-RE.
17. Rattanakreetakul, C.; Keawmanee, P.; Bincader, S.; Mongkolporn, O.; Phuntumart, V.; Chiba, S.; Pongpisutta, R. Two newly identified Colletotrichum species associated with mango anthracnose in central Thailand. *Plants* **2023**, *12*, 1130, doi:https://doi.org/10.3390/plants12051130.
18. Lin, W.-L.; Duan, C.-H.; Wang, C.-L. Identification and virulence of *Colletotrichum* species causing anthracnose on mango. *Plant Pathology* **2022**, *72*, doi:https://doi.org/10.1111/ppa.13682.
19. Damm, U.; Cannon, P.; Woudenberg, J.H.C.; Crous, P.W. The Colletotrichum acutatum species complex. *Studies in Mycology* **2012**, *73*, 37-113, doi:https://doi.org/10.3114/sim0010.
20. Freeman, S.; Katan, T.; Shabi, E. Characterization of Colletotrichum species responsible for anthracnose diseases of various fruits. *Plant Disease* **2007**, *82*, doi:https://doi.org/10.1094/PDIS.1998.82.6.596.
21. Sharma, G.; Gryzenhout, M.; Hyde, K.D.; Pinnaka, A.K.; Shenoy, B.D. First report of Colletotrichum asianum causing mango anthracnose in South Africa. *Plant Disease* **2013**, *99*, doi:https://doi.org/10.1094/PDIS-08-13-0837-PDN.
22. Sharma, G.; Kumar, N. Mango Anthracnose: A Review. *Asian Journal of Agricultural and Horticultural Research* **2021**, *5*, 47-55.
23. Matulaprungsan, B.; Wongs-Aree, C.; Penchaiya, P.; Boonyaritthongchai, P.; Srisurapanon, V.; Kanlayanarat, S. Analysis of Critical Control Points of Post-Harvest Diseases in the Material Flow of Nam Dok Mai Mango Exported to Japan. *Agriculture* **2019**, *9*, 200, doi:https://doi.org/10.3390/agriculture9090200.
24. Li, Q.; Bu, J.; Shu, J.; Yu, Z.; Tang, L.; Huang, S.; Guo, T.; Mo, J.; Luo, S.; Solangi, G.S.; et al. Colletotrichum species associated with mango in southern China. *Scientific Reports* **2019**, *9*, 18891, doi:https://doi.org/10.1038/s41598-019-54809-4.
25. Dinh, S.-Q.; Chongwungse, J.; Pongam, P.; Sangchote, S. Fruit infection by Colletotrichum gloeosporioides and anthracnose resistance of some mango cultivars in Thailand. *Australasian Plant Pathology* **2003**, *32*, doi:https://doi.org/10.1071/AP03053.
26. Ganesan, S.; Kumari, N.; Sahu, S.; Pattanaik, M.; Raj, A.; Panda, M.; Srinivas, P.; Singh, H.S. Characterization of Colletotrichum species causing new pre-harvest anthracnose symptoms on mango in Eastern India. *Australasian Plant Pathology* **2024**, *53*, 239–252, doi:https://doi.org/10.1007/s13313-024-00973-9.
27. Pujari, J.D.; Yakkundimath, R. Grading and classification of anthracnose fungal disease of fruits based on statistical texture features. *Environmental Science* **2013**, *52*, 121-132.
28. Dofuor, A.K.; Quartey, N.K.-A.; Osabutey, A.F.; Antwi-Agyakwa, A.K.; Asante, K.; Boateng, B.O.; Ablormeti, F.K.; Lutuf, H.; Osei-Owusu, J.; Osei, J.H.N.; et al. Mango anthracnose disease: the current situation and direction for future research. *Frontiers in Microbiology* **2023**, *14*, doi:https://doi.org/10.3389/fmicb.2023.1168203.
29. Siripatrawan, U.; Makino, Y. Hyperspectral imaging coupled with machine learning for classification of anthracnose infection on mango fruit. *Spectrochimica Acta Part A: Molecular and Biomolecular Spectroscopy* **2024**, *309*, 123825, doi:https://doi.org/10.1016/j.saa.2023.123825.
30. Velásquez, C.; Aleixos, N.; Gomez-Sanchis, J.; Cubero, S.; Prieto, F.; Blasco, J. Enhancing anthracnose detection in mango at early stages using hyperspectral imaging and machine learning. *Postharvest Biology and Technology* **2024**, *209*, 112732, doi:https://doi.org/10.1016/j.postharvbio.2023.112732.
31. Velásquez, C.; Prieto, F.; Palou, L.; Cubero, S.; Blasco, J.; Aleixos, N. New model for the automatic detection of anthracnose in mango fruits based on vis/nir hyperspectral imaging and discriminant analysis. *Journal of Food Measurement and Characterization* **2024**, *18*, 560–570, doi:https://doi.org/10.1007/s11694-023-02173-3.
32. Food and Agriculture Organization of the United Nations. Thai Agricultural Standard (TAS 5-2015)-Mongo. **2015**.
33. Sharma, S.; K.C., S.; Sirisomboon, P. Rapid ripening stage classification and dry matter prediction of durian pulp using a pushbroom near infrared hyperspectral imaging system. *Measurement* **2022**, *189*, 110464, doi:https://doi.org/10.1016/j.measurement.2021.110464.
34. Tsai, C.-M.; Guan, S.-S. Identifying regions of interest in reading an image. *Displays* **2015**, *39*, 33-41, doi:https://doi.org/10.1016/j.displa.2015.08.001.
35. Williams, P.; Manley, M.; Antoniszyn, J. *Near-infrared Technology: Getting the Best Out of Light*; SUN PReSS: South Africa, 2019.
36. Liu, Y.; Zhou, S.; Han, W.; Liu, W.; Qiu, Z.; Li, C. Convolutional neural network for hyperspectral data analysis and effective wavelengths selection. *Analytica Chimica Acta* **2019**, *1086*, 46-54, doi:https://doi.org/10.1016/j.aca.2019.08.026.

Preprints.org (www.preprints.org) | NOT PEER-REVIEWED | Posted: 12 August 2024 doi:10.20944/preprints202408.0759.v1

37. Chung, H.; Wi, S.; Cho, B.-K.; Lee, d. Classification of Garlic (Allium sativum L.) Crops by Fertilizer Differences Using Ground-Based Hyperspectral Imaging System. *Agriculture* **2024**, *14*, 1215, doi:https://doi.org/10.3390/agriculture14081215.
38. Fazari, A.; Pellicer-Valero, O.J.; Gómez-Sanchıs, J.; Bernardi, B.; Cubero, S.; Benalia, S.; Zimbalatti, G.; Blasco, J. Application of deep convolutional neural networks for the detection of anthracnose in olives using VIS/NIR hyperspectral images. *Computers and Electronics in Agriculture* **2021**, *187*, 106252, doi:https://doi.org/10.1016/j.compag.2021.106252.
39. Lu, J.; Ehsani, R.; Shi, Y.; Abdulridha, J.; Castro, A.I.d.; Xu, Y. Field detection of anthracnose crown rot in strawberry using spectroscopy technology. *Computers and Electronics in Agriculture* **2017**, *135*, 289-299, doi:https://doi.org/10.1016/j.compag.2017.01.017.
40. Amirruddin, A.D.; Muharam, F.M.; Ismail, M.H.; Ismail, M.F.; Tan, N.P.; Karam, D.S. Hyperspectral remote sensing for assessment of chlorophyll sufficiency levels in mature oil palm (Elaeis guineensis) based on frond numbers: Analysis of decision tree and random forest. *Computers and Electronics in Agriculture* **2020**, *169*, 105221, doi:https://doi.org/10.1016/j.compag.2020.105221.
41. Jensen, J.R. *Introductory Digital Image Processing: A Remote Sensing Perspective*; Prentice Hall Press: Upper Saddle River, NJ, USA, 2005.

Disclaimer/Publisher's Note: The statements, opinions and data contained in all publications are solely those of the individual author(s) and contributor(s) and not of MDPI and/or the editor(s). MDPI and/or the editor(s) disclaim responsibility for any injury to people or property resulting from any ideas, methods, instructions or products referred to in the content.